

Understanding Error Propagation in Deep Learning Neural Network (DNN) Accelerators and Applications

Guanpeng Li

University of British Columbia
gpli@ece.ubc.ca

Siva Kumar Sastry Hari
NVIDIA
shari@nvidia.com

Michael Sullivan
NVIDIA
misullivan@nvidia.com

Timothy Tsai
NVIDIA
timothytsai@nvidia.com

Karthik Pattabiraman
University of British Columbia
karthikp@ece.ubc.ca

Joel Emer
NVIDIA
jemer@nvidia.com

Stephen W. Keckler
NVIDIA
skeckler@nvidia.com

ABSTRACT

Deep learning neural networks (DNNs) have been successful in solving a wide range of machine learning problems. Specialized hardware accelerators have been proposed to accelerate the execution of DNN algorithms for high-performance and energy efficiency. Recently, they have been deployed in datacenters (potentially for business-critical or industrial applications) and safety-critical systems such as self-driving cars. Soft errors caused by high-energy particles have been increasing in hardware systems, and these can lead to catastrophic failures in DNN systems. Traditional methods for building resilient systems, e.g., Triple Modular Redundancy (TMR), are agnostic of the DNN algorithm and the DNN accelerator's architecture. Hence, these traditional resilience approaches incur high overheads, which makes them challenging to deploy. **In this paper, we experimentally evaluate the resilience characteristics of DNN systems (i.e., DNN software running on specialized accelerators). We find that the error resilience of a DNN system depends on the data types, values, data reuses, and types of layers in the design. Based on our observations, we propose two efficient protection techniques for DNN systems.**

KEYWORDS

Deep Learning, Silent Data Corruption, Soft Error, Reliability

ACM Reference Format:

Guanpeng Li, Siva Kumar Sastry Hari, Michael Sullivan, Timothy Tsai, Karthik Pattabiraman, Joel Emer, and Stephen W. Keckler. 2017. Understanding Error Propagation in Deep Learning Neural Network (DNN) Accelerators and Applications. In *Proceedings of SC17*. ACM, Denver, CO, USA, 12 pages. <https://doi.org/10.1145/3126908.3126964>

Permission to make digital or hard copies of all or part of this work for personal or classroom use is granted without fee provided that copies are not made or distributed for profit or commercial advantage and that copies bear this notice and the full citation on the first page. Copyrights for components of this work owned by others than ACM must be honored. Abstracting with credit is permitted. To copy otherwise, or republish, to post on servers or to redistribute to lists, requires prior specific permission and/or a fee. Request permissions from permissions@acm.org.

SC17, November 12–17, 2017, Denver, CO, USA
© 2017 Association for Computing Machinery.
ACM ISBN 978-1-4503-5114-0/17/11...\$15.00
<https://doi.org/10.1145/3126908.3126964>

1 INTRODUCTION

Deep learning neural network (DNN) applications are widely used in high-performance computing systems and datacenters [4, 18, 47]. Researchers have proposed the use of specialized hardware accelerators to accelerate the inferencing process of DNNs, consisting of thousands of parallel processing engines [12, 14, 25]. For example, Google recently announced its DNN accelerator, the Tensor Processing Unit (TPU), which they deploy in their datacenters for DNN applications [58].

While the performance of DNN accelerators and applications have been extensively studied, the reliability implications of using them is not well understood. One of the major sources of unreliability in modern systems are soft errors, typically caused by high-energy particles striking electronic devices and causing them to malfunction (e.g., flip a single bit) [5, 16]. Such soft errors can cause application failures, and they can result in violations of safety and reliability specifications. For example, the IEC 61508 standard [28] provides reliability specifications for a wide range of industrial applications ranging from the oil and gas industry to nuclear power plants. Deep neural networks have promising uses for data analytics in industrial applications [60], but they must respect the safety and reliability standards of the industries where they are employed.

A specific and emerging example of HPC DNN systems is for self-driving cars (i.e., autonomous vehicles), which deploy high performance DNNs for real-time image processing and object identification. The high performance, low power, high reliability, and real-time requirements of these applications require hardware that rivals that of the fastest and most reliable supercomputer (albeit with lower precision and memory requirements). **For instance, NVIDIA Xavier—a next-generation SoC with a focus on self-driving applications—is expected to deliver 20 Tops/s at 20W in 16nm technology [51].** We focus our investigation into DNN systems¹ in this emerging HPC market due to its importance, stringent reliability requirements, and its heavy use of DNNs for image analysis. **The ISO 26262 standard for functional safety of road vehicles mandates the overall FIT rate² of the System on Chip (SoC) carrying the DNN**

¹We use the term DNN systems to refer to both the software and the hardware accelerator that implements the DNN.

²Failure-in-Time rate: 1 FIT = 1 failure per 1 billion hours

inferencing hardware under soft errors to be less than 10 FIT [48]. This requires us to measure and understand the error resilience characteristics of these high-performance DNN systems.

This paper takes a first step towards this goal by (1) characterizing the propagation of soft errors from the hardware to the application software of DNN systems, and (2) devising cost-effective mitigation mechanisms in both software and hardware, based on the characterization results

Traditional methods to protect computer systems from soft errors typically replicate the hardware components (e.g., Triple Modular Redundancy or TMR). While these methods are useful, they often incur large overheads in energy, performance and hardware cost. This makes them very challenging to deploy in self-driving cars, which need to detect objects such as pedestrians in real time [33] and have strict cost constraints. To reduce overheads, researchers have investigated software techniques to protect programs from soft errors, e.g., identifying vulnerable static instructions and selectively duplicating the instructions [20, 26, 35]. The main advantage of these techniques is that they can be tuned based on the application being protected. However, DNN software typically has a very different structure compared to general-purpose software. For example, the total number of static instruction types running on the DNN hardware is usually very limited (less than five) as they are repeatedly executing the multiply-accumulate (MAC) operations. This makes these proposed techniques very difficult to deploy as duplicating even a single static instruction will result in huge overheads. Thus, current protection techniques are DNN-agnostic in that they consider neither the characteristics of DNN algorithms, nor the architecture of hardware accelerators. To the best of our knowledge, we are the first to study the propagation of soft errors in DNN systems and devise cost-effective solutions to mitigate their impact.

We make the following major contributions in this paper:

- We modify a DNN simulator to inject faults in four widely used neural networks (AlexNet, CaffeNet, NiN and ConvNet) for image recognition, using a canonical model of the DNN accelerator hardware.
- We perform a large-scale fault injection study using the simulator for faults that occur in the data-path of accelerators. We classify the error propagation behaviors based on the structure of the neural networks, data types, positions of layers, and the types of layers.
- We use a recently proposed DNN accelerator, Eyeriss [13], to study the effect of soft errors in different buffers and calculate its projected FIT rates.
- Based on our observations, we discuss the reliability implications of designing DNN accelerators and applications and also propose two cost-effective error protection techniques to mitigate Silent Data Corruptions (SDCs) i.e., incorrect outcomes. The first technique, symptom-based detectors, is implemented in software and the second technique, selective latch hardening, in hardware. We evaluate these techniques with respect to their fault coverage and overhead.

Our main results and implications are as follows:

- We find that different DNNs have different sensitivities to SDCs depending on the topology of the network, the data type used, and the bit position of the fault. In particular, we find that only high-order bits are vulnerable to SDCs, and the vulnerability

is proportional to the dynamic value range the data type can represent. The implications of this result are twofold: (1) When designing DNN systems, one should choose a data type providing just-enough dynamic value range and precision. The overall FIT rate of the DNN system can be reduced by more than an order of magnitude if we do so - this is in line with recent work that has proposed the use of such data types for energy efficiency. (2) Leveraging the asymmetry of the SDC sensitivity of bits, we can selectively protect the vulnerable bits using our proposed selective latch hardening technique. Our evaluation shows that the corresponding FIT rate of the datapath can be reduced by 100x with about 20% area overhead.

- We observe that faults causing a large deviation in magnitude of values likely lead to SDCs. Normalization layers can reduce the impact of such faults by averaging the faulty values with adjacent correct values, thereby mitigating SDCs. While the normalization layers are typically used to improve performance of a DNN, they also boost its resilience. Based on the characteristics, we propose a symptom-based detector that provides 97.84% precision and 92.08% recall in error detection, for selected DNNs and data types.
- In our case study of Eyeriss, the sensitivity study of each hardware component shows that some buffers implemented to leverage data locality for performance may dramatically increase the overall FIT rate of a DNN accelerator by more than 100x. This indicates that novel dataflows proposed in various studies should also add protection to these buffers as they may significantly degrade the reliability otherwise.
- Finally, we find that for the Eyeriss accelerator platform, the FIT rates can exceed the safety standards (i.e., ISO 26262) by orders of magnitude without any protection. However, applying the proposed protection techniques can reduce the FIT rate considerably and restore it within the safety standards.

2 BACKGROUND

2.1 Deep Learning Neural Networks

A deep learning neural network (DNN) is a directed acyclic graph consisting of multiple computation layers [34]. A higher level abstraction of the input data or a feature map (fmap) is extracted to preserve the information that are unique and important in each layer. There is a very deep hierarchy of layers in modern DNNs, and hence their name.

We consider convolutional neural networks of DNNs, as they are used in a broad range of DNN applications and deployed in self-driving cars, which are our focus. In such DNNs, the primary computation occurs in the convolutional layers (CONV) that perform multi-dimensional convolution calculations. The number of convolutional layers can range from three to a few tens of layers [27, 31]. Each convolutional layer applies a kernel (or filter) on the input fmaps (ifmaps) to extract underlying visual characteristics and generate the corresponding output fmaps (ofmaps).

Each computation result is saved in an activation (ACT) after being processed by an activation function (e.g., ReLU), which is in turn, the input of the next layer. An activation is also known as a neuron or a synapse - in this work, we use ACT to represent an activation. ACTs are connected based on the topology of the network. For example, if two ACTs, A and B, are both connected to an ACT C



in the next layer, then ACT C is calculated using ACT A and B as the inputs. In convolutional layers, ACTs in each fmap are usually fully connected to each other, whereas the connection of ACTs between each fmap in other layers are usually sparse. In some DNNs, a small number (usually less than 3) of fully-connected layers (FC) are typically stacked behind the convolutional layers for classification purposes. In between the convolutional and fully-connected layers, additional layers can be added, such as the pooling (POOL) and normalization (NORM) layers. POOL selects the ACT of the local maximum in an area to be forwarded to the next layer and discards the rest in the area, so the size of fmaps will become smaller after each POOL. NORM averages ACT values based on the surrounding ACTs. Thus ACT values will also be modified after the NORM layer.

Once a DNN topology is constructed, the network can be fed with training input data, and the associated weights, abstracted as connections between ACTs, will be learned through a back-propagation process. This is referred to as the *training* phase of the network. The training is usually done once, as it is very time-consuming, and then the DNN is ready for image classification with testing input data. This is referred to as the *inferencing* phase of the network and is carried out many times for each input data set. The input of the inferencing phase is often a digitized image, and the output is a list of output candidates of possible matches such as *car, pedestrian, animal*, each with a confidence score. Self-driving cars deploy DNN applications for inferencing, and hence, we focus on the inferencing phase of DNNs.

2.2 DNN Accelerator

Many specialized accelerators [12, 13, 25] have been proposed for DNN inferencing, each with different features to cater to DNN algorithms. However, there are two properties common to all DNN algorithms that are used in the design of all DNN accelerators: (1) MAC operations in each feature map have very sparse dependencies, which can be computed in parallel, and (2) there are strong temporal and spatial localities in data within and across each feature map, which allow the data to be strategically cached and reused. To leverage the first property, DNN accelerators adopt spatial architectures [57], which consist of massively parallel processing engines (PEs), each of which computes MACs. Figure 1 shows the architecture of a general DNN accelerator. A DNN accelerator consists of a global buffer and an array of PEs. The accelerator is connected to DRAM where data is transferred from. A CPU is usually used to off-load tasks to the accelerator. The overall architecture is shown in Figure 1a. The ALU of each PE consists of a multiplier and an adder as execution units to perform MACs — this is where the majority of computations happen in DNNs. A general structure of the ALU in each PE is shown in Figure 1b.

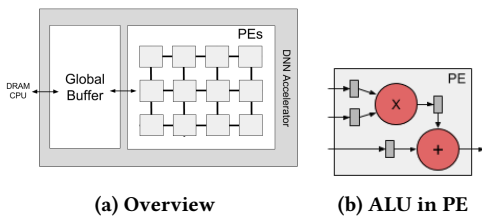


Figure 1: Architecture of general DNN accelerators

To leverage the second property of DNN algorithms, special buffers are added on each PE as local scratchpad to cache data for reuse. Each DNN accelerator may implement its own dataflow to explore data localities. We classify the localities in DNNs into three major categories:

- **Weight Reuse:** Weight data of each kernel can be reused in each fmap as the convolutions involving the kernel data are used many times on the same ifmap.
- **Image Reuse:** Image data of each fmap can be reused in all convolutions where the ifmap is involved, because different kernels operate on the same sets of ifmap in each layer.
- **Output Reuse:** Computation results of MACs can be buffered and consumed on-PE without transferring off the PEs.

Table 1 illustrates nine different DNN accelerators that have been proposed in prior work and the corresponding data localities they exploit in their dataflows. As can be seen, each accelerator exploits one of more localities in its dataflow. Eyeriss [13] considers all of the three data localities in its dataflow.

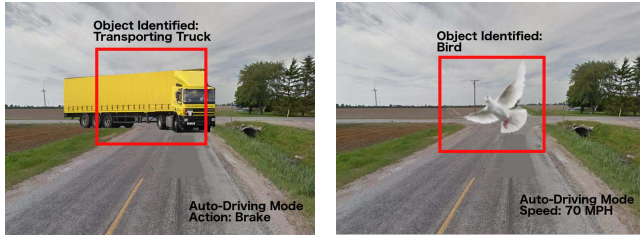
We separate faults that originate in the datapath (i.e., latches in execution units) from those that originate in buffers (both on- and off-PEs), because they propagate differently: faults in the datapath will be only read once, whereas faults in buffers may be read multiple times due to reuse and hence the same fault can be spread to multiple locations within short time windows.

Table 1: Data Reuses in DNN Accelerators

Accelerators	Weight Reuse	Image Reuse	Output Reuse
Zhang et al. [61], Diannao [12], Dadiannao [14]	x	x	x
Chakradhar et al. [10], Sriram et al. [53], Sankaradas et al. [49], nn-X [23], K-Brain [41], Origami [9]	✓	x	x
Gupta et al. [24], Shidiannao [19], Peemen et al. [43]	x	x	✓
Eyeriss [13]	✓	✓	✓

2.3 Consequences of Soft Errors

The consequences of soft errors that occur in DNN systems can be catastrophic as many of them are safety-critical, and error mitigation is required to meet certain reliability targets. For example, in self-driving cars, a soft error can lead to misclassification of objects, resulting in a wrong action taken by the car. In our fault injection experiments, we found many cases where a truck can be misclassified under a soft error. We illustrate this in Figure 2. The DNN in the car should classify the coming object as a transporting truck in a fault-free execution and apply the brakes in time to avoid a collision (Figure 2a). However, due to a soft error in the DNN, the truck is misclassified as a bird (Figure 2b), and the braking action may not be applied in time to avoid the collision, especially when the car is operating at high speed. This is an important concern as it often results in the violation of standards such as ISO 26262 dealing with the functional safety of road vehicles [48], which requires the System on Chip (SoC) carrying DNN inferencing hardware in self-driving cars to have a soft error FIT rate less than 10 FIT [2], regardless of the underlying DNN algorithm and accuracy. Since a DNN accelerator is only a fraction of the total area of the SoC, the FIT allowance of a DNN accelerator should be much lower than 10 in self-driving cars. However, we find that a DNN accelerator alone may exceed the total required FIT rate of the SoC without protection (Section 5.2).



(a) Fault-free execution: A truck is identified by the DNN and brakes are applied (b) SDC: Truck is incorrectly identified as bird and brakes may not be applied

Figure 2: Example of SDC that could lead to collision in self-driving cars due to soft errors

3 EXPLORATION OF DESIGN SPACE

We seek to understand how soft errors that occur in DNN accelerators propagate in DNN applications and cause SDCs (we define SDCs later in Section 4.6). We focus on SDCs as these are the most insidious of failures and cannot be detected easily. There are four parameters that impact of soft errors on DNNs:

(1) **Topology and Data Type:** Each DNN has its own distinct topology which affects error propagation. Further, DNNs can also use different data types in their implementation. We want to explore the effect of the topology and data type on the overall SDC probability.

(2) **Bit Position and Value:** To further investigate the impact of data type on error propagation, we examine the sensitivity of each bit position in the networks using different data types. This is because the values represented by a data type depend on the bit positions affected, as different data types interpret each bit differently (explained in Section 4.5). Hence, we want to understand how SDC probabilities vary based on the bit corrupted in each data type and how the errors result in SDCs affect program values.

(3) **Layers:** Different DNNs have different layers - this includes the differences in type, position, and the total number of layers. We investigate how errors propagate in different layers and whether the propagation is influenced by the characteristics of each layer.

(4) **Data Reuse:** We want to understand how different data reuses implemented in the dataflows of DNN accelerators affects the SDC probability. Note that unlike other parameters, data reuse is not a property of the DNN itself but of its hardware implementation.

4 EXPERIMENTAL SETUP

4.1 Networks

Table 2: Networks Used

Network	Dataset	No. of Output Candidates	Topology
ConvNet [17]	CIFAR-10	10	3 CONV + 2 FC
AlexNet [31]	ImageNet	1,000	5 CONV(with LRN) + 3 FC
CaffeNet [8]	ImageNet	1,000	5 CONV(with LRN) + 3 FC
NiN [37]	ImageNet	1,000	12 CONV

We focus on convolutional neural networks in DNNs, as they have shown great potential in solving many complex and emerging

problems and are often executed in self-driving cars. There are four neural networks that we consider in Table 2. They range from the relatively simple 5-layer ConvNet to the 12-layer NiN. The reasons we chose these networks are: (1) They have different topologies and methods implemented to cover a variety of common features used in today's DNNs, and the details are publicly accessible, (2) they are often used as benchmarks in developing and testing DNN accelerators [13, 30, 52], and (3) they are well known to solve challenging problems, (4) and the official pre-trained models are freely available. This allows us to fully reproduce the networks for benchmarking purposes. All of the networks perform the same task, namely image classification. We use the ImageNet dataset [29] for AlexNet, CaffeNet and NiN, and the CIFAR-10 dataset [15] for ConvNet, as they were trained and tested with these datasets. We use these reference datasets and the pre-trained weights together with the corresponding networks from the Berkeley Vision and Learning Center (BVLC) [6].

We list the details of each network in Table 2. As shown, all networks except NiN have fully-connected layers behind the convolutional layers. All four networks implement ReLU as the activation function and use the max-pooling method in their sub-sampling layers. Both AlexNet and CaffeNet use a Local Response Normalization (LRN) layer following each of the first two convolutional layers - the only difference is the order of the ReLU and the sub-sampling layer in each convolution layer. In AlexNet, CaffeNet and ConvNet, there is a soft-max layer at the very end of each network to derive the confidence score of each ranking, which is also part of the network's output. However, in NiN, there is no such soft-max layer. Hence, the output of the NiN network has only the ranking of each candidate without their confidence scores.

4.2 DNN Accelerators

We consider nine of DNN accelerators mentioned in Table 1. We separate the faults in the datapaths of the networks from those in the buffers. We study datapath faults based on the common abstraction of their execution units in Figure 1b. Thus, the results for datapath faults apply to all nine accelerators.

For buffer faults, since the dataflow (and buffer structure) is different in each accelerator, we have to choose a specific design. We chose the Eyeriss accelerator for studying buffer faults because: (1) The dataflow of Eyeriss includes all three data localities in DNNs listed in Table 1, which allows us to study the data reuse seen in other DNN accelerators, and (2) the design parameters of Eyeriss are publicly available, which allows us to conduct a comprehensive analysis on its dataflow and overall resilience.

4.3 Fault Model

We consider transient, single-event upsets that occur in the datapath and buffers, both inside and outside the processing engines of DNN accelerators. We do not consider faults that occur in combinational logic elements as they are much less sensitive to soft errors than storage elements shown in recent studies [22, 50]. We also do not consider errors in control logic units. This is due to the nature of DNN accelerators which are designed for offloaded data acceleration - the scheduling is mainly done by the host (i.e., CPU). Finally,

because our focus is on DNN accelerators, we do not consider faults in the CPU, main memory, or the memory/data buses.

4.4 Fault Injection Simulation

Since we do not have access to the RTL implementations of the accelerators, we use a DNN simulator for fault injection. We modified an open-source DNN simulator framework, Tiny-CNN [56], which accepts Caffe pre-trained weights [7] of a network for inferencing and is written in C++. We map each line of code in the simulator to the corresponding hardware component, so that we can pinpoint the impact of the fault injection location in terms of the underlying microarchitectural components. We randomly inject faults in the hardware components we consider by corrupting the values in the corresponding executions in the simulator. This fault injection method is in line with other related work [26, 32, 35, 36, 59].

4.5 Data Types

Different data types offer different tradeoffs between energy consumption and performance in DNNs. Our goal is to investigate the sensitivity of different design parameters in data types to error propagation. Therefore, we selected a wide range of data types that have different design parameters as listed in Table 3. We classify them into two types: floating-point data type (FP) and fixed-point data type (FxP). For FP, we choose 64-bit double, 32-bit float, and 16-bit half-float, all of which follow the IEEE 754 floating-point arithmetic standard. We use the terms DOUBLE, FLOAT, and FLOAT16 respectively for these FP data types in this study. For FxPs, unfortunately there is no public information about how binary points (radix points) are chosen for specific implementations. Therefore, we choose different binary points for each FxP. We use the following notations to represent FxPs in this work: 16b_rb10 means a 16-bit integer with 1 bit for the sign, 5 bits for the integer part, and 10 bits for the mantissa, from the leftmost bit to the rightmost bit. We consider three FxP types, namely 16b_rb10, 32b_rb10 and 32b_rb26. They all implement 2's complement for their negative arithmetic. Any value that exceeds the maximum or minimum dynamic value range will be saturated to the maximum or minimum value respectively.

Table 3: Data types used

Data Type	FP or FxP	Data Width	Bits (From left to right)
DOUBLE	FP	64-bit	1 sign bit, 11 bits for exponent, 52 bits for mantissa
FLOAT	FP	32-bit	1 sign bit, 8 bits for exponent, 23 bits for mantissa
FLOAT16	FP	16-bit	1 sign bit, 5 bits for exponent, 10 bits for mantissa
32b_rb26	FxP	32-bit	1 sign bit, 5 bits for integer, 26 bits for mantissa
32b_rb10	FxP	32-bit	1 sign bit, 21 bits for integer, 10 bits for mantissa
16b_rb10	FxP	16-bit	1 sign bit, 5 bits for integer, 10 bits for mantissa

4.6 Silent Data Corruption (SDC)

We define the SDC probability as the probability of an SDC given that the fault affects an architecturally visible state of the program (i.e., the fault was activated). This is in line with the definition used in other work [20, 26, 36, 59].

In a typical program, an SDC would be a failure outcome in which the application's output deviates from the correct (golden) output. This comparison is typically made on a bit-by-bit basis. However, for DNNs, there is often not a single correct output, but a list of ranked outputs each with a confidence score as described in Section 2.1, and

hence a bit-by-bit comparison would be misleading. Consequently, we need to define new criteria to determine what constitutes an SDC for a DNN application. We define four kinds of SDCs as follows:

- SDC-1: The top ranked element predicted by the DNN is different from that predicted by its fault-free execution. This is the most critical SDC because the top-ranked element is what is typically used for downstream processing.
- SDC-5: The top ranked element is not one of the top five predicted elements of the fault-free execution of the DNN.
- SDC-10%: The confidence score of the top ranked element varies by more than +/-10% of its fault-free execution.
- SDC-20%: The confidence score of the top ranked element varies by more than +/-20% of its fault-free execution.

4.7 FIT Rate Calculation

The formula of calculating the FIT rate of a hardware structure is shown in Equation 1, where R_{raw} is the raw FIT rate (estimated as 20.49 FIT/Mb by extrapolating the results of Neale et al. [39]. The original measurement for a 28nm process is 157.62 FIT/MB in the paper. We project this for a 16nm process by applying the trend shown in Figure 1 of the Neale paper³). $S_{component}$ is the size of the component, and $SDC_{component}$ is the SDC probability of each component. We use this formula to calculate the FIT rate of datapath components and buffer structures of DNN accelerators, as well as the overall FIT rate of Eyeriss in Section 5.1 and Section 5.2.

$$FIT = \sum_{component} R_{raw} * S_{component} * SDC_{component} \quad (1)$$

5 CHARACTERIZATION RESULTS

We organize the results based on the origins of faults (i.e., datapath faults and buffer faults) for each parameter. We randomly injected 3,000 faults per latch, one fault for each execution of the DNN application. The error bars for all the experimental results are calculated based on 95% confidence intervals.

5.1 Datapath Faults

5.1.1 Data Types and Networks. Figure 3 shows the results of the fault injection experiments on different networks and different data types. We make three observations based on the results.

First, SDC probabilities vary across the networks for the same data type. For example, using the FLOAT data type, the SDC probabilities for NiN are higher than for other networks using the same data type (except ConvNet - see reason below). This is because of the different structures of networks in terms of sub-sampling and normalization layers which provide different levels of error masking - we further investigate this in Section 5.1.4. Further, ConvNet has the highest SDC propagation probabilities among all the networks considered (we show the graph for ConvNet separately as its SDC probabilities are significantly higher than the other networks). This is because the structure of ConvNet is much less deep than for other networks, and consequently there is higher error propagation in ConvNet. For example, there are only 3 convolutional layers

³We also adjusted the original measurement by a factor of 0.65 as there is a mistake we found in the paper. The authors of the paper have acknowledged the mistake in private email communications with us.

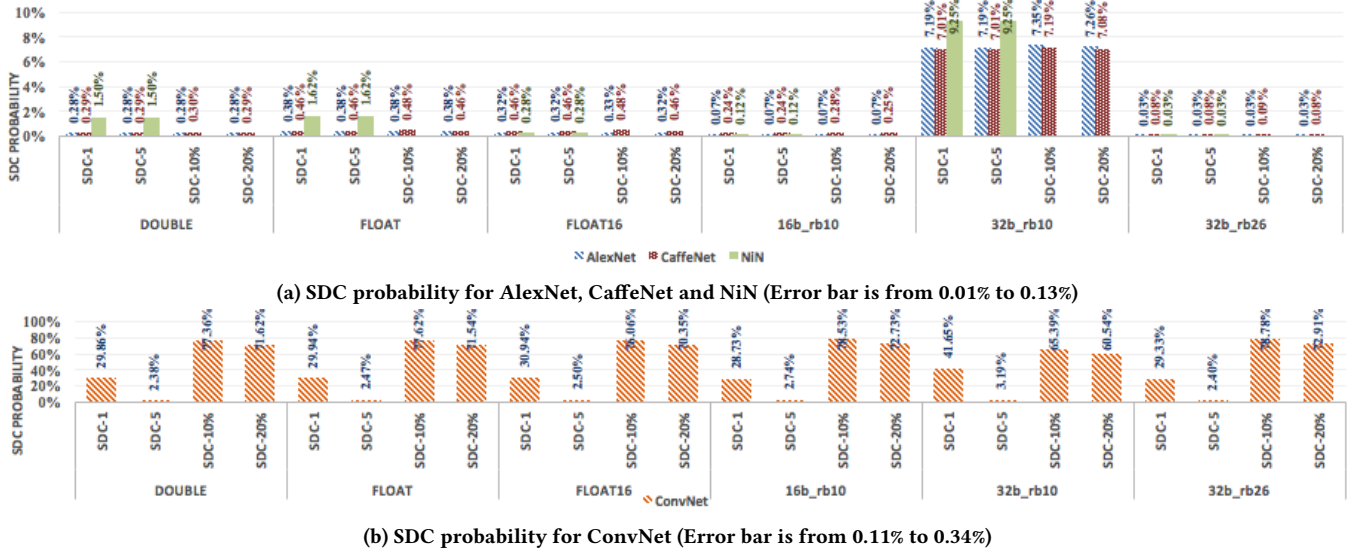


Figure 3: SDC probability for different data types in different networks (for faults in PE latches).

in ConvNet, whereas there are 12 in NiN. Further, ConvNet does not have normalization layers to provide additional error masking, unlike AlexNet and CaffeNet.

Second, SDC probabilities vary considerably across data types. For instance, in AlexNet, SDC-1 can be as high as 7.19% using 32b_rb10, and as low as 0.38% using FLOAT - the maximum difference is 240x (between SDC-1 in 32b_rb10 and 32b_rb26). The reasons are further explored in Section 5.1.2.

Finally, for networks using the ImageNet dataset (all except ConvNet), there is little difference in the SDC probability for the four different kinds of SDCs for a particular network and data type. Recall that there are 1,000 output dimensions in the ImageNet DNNs. If the top ranked output is changed by the error, the new ranking is likely to be outside of the top five elements, and its confidence score will likely change by more than 20%. However, in ConvNet, which uses the CIFAR-10 dataset, the four SDC probabilities are quite different. This is because there are only 10 output dimensions in ConvNet, and if the top ranked output is affected by errors, it is still highly likely to stay within the top five elements. As a result, the SDC-5 probability is quite low for this network. On the other hand, the SDC-10% and SDC-20% probabilities are quite high in ConvNet compared to the other networks, as the confidence scores are more sensitive due to the small output dimensions compared to the other networks. Note that since NiN does not provide confidence scores in its output, we do not show SDC-10% and SDC-20% for NiN.

Because there is little difference between the SDC types for three of the four networks, we focus on SDC-1 in the rest of the paper and refer to them as SDCs unless otherwise specified.

5.1.2 Bit Position. We show the results by plotting the SDC probabilities for each bit in each data type. Due to space constraints, we only show the results for NiN using FLOAT and FLOAT16 data types for FP, and for CaffeNet using 32b_rb26 and 32b_rb10 for FxP. We however confirmed that similar observations apply to the rest of networks and data types.

The results of NiN using FLOAT and FLOAT16 are shown in Figure 4a and Figure 4b respectively. For the FP data types, only the high-order exponent bits are likely to cause SDCs (if corrupted), and not the mantissa and sign bits. We also observed that bit-flips that go from 0 to 1 in the high-order exponent bits are more likely to cause SDCs than those that go from 1 to 0. This is because the correct values in each network are typically clustered around 0 (see Section 5.1.3) and hence, small deviations in the magnitude or sign bits do not matter as much. This is also why the per-bit SDC probability for FLOAT16 is lower than that for FLOAT. A corrupted bit in the exponent of the latter is likely to cause a larger deviation from 0, which in turn is likely to result in an SDC.

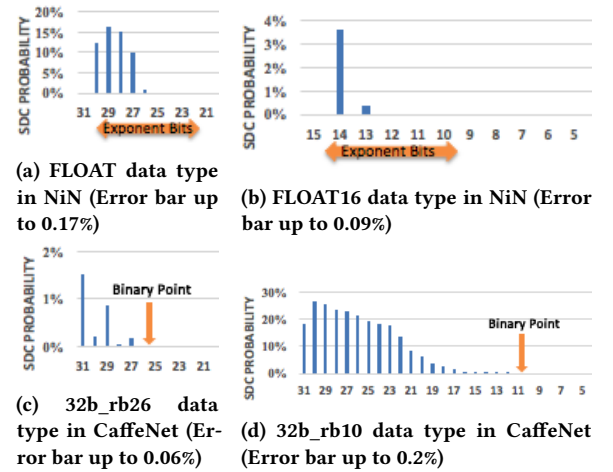
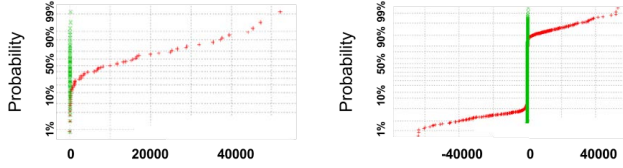


Figure 4: SDC probability variation based on bit position corrupted, bit positions not shown have zero SDC probability (Y-axis is SDC probability and X-axis is bit position)

For FxP data types, we plot the results for CaffeNet using 32b_rb26 and 32b_rb10 in Figure 4c and Figure 4d respectively. As can be seen, only bits in the integer parts of the fixed point data types are vulnerable. Both FxP data types have 32-bit data widths but different binary point positions. We observed that the per-bit SDC probability for the data type 32b_rb10 is much higher than that of 32b_rb26. For example, the 30th bit in 32b_rb10 has an SDC probability of 26.65% whereas the same bit position only has an SDC probability of 0.22% in 32b_rb26. This is because 32b_rb26 has a smaller dynamic range of values compared to 32b_rb10, and hence the corrupted value in the former is likely to be closer to 0 than the latter. This is similar to the FP case above.

5.1.3 Value. We chose AlexNet using FLOAT16 to explain how errors that result in SDCs affect program values. We randomly sampled the set of ACTs in the network that were affected by errors, and compared their values before (in green) and after (in red) error occurrence. We classified the results based on whether the errors led to SDCs (Figure 5a) or were benign (Figure 5b). There are two key observations: (1) If an error causes a large deviation in numeric values, it likely causes an SDC. For example, in Figure 5a, more than 80% of errors that lead to a large deviation lead to an SDC. (2) In Figure 5b, on the other hand, only 2% of errors that cause large deviations result in benign faults. This is likely because large deviations make it harder for values in the network to converge back to their correct values which are typically clustered around 0.



(a) Values before (green dots) and after (red dots) errors resulting in SDCs. X-axis represents values. (b) Values before (green dots) and after (red dots) errors resulting in benign. X-axis represents values.

Figure 5: Values before and after error occurrence in AlexNet using FLOAT16

We now ask the following questions. How close together are the correct (error-free) values in each network, and how much do the erroneous values deviate from the correct ones? Answering these questions will enable us to formulate efficient error detectors. We list boundary values of ACTs profiled in each layer and network in Table 4. As can be seen, in each network and layer, the values are bounded within a relatively small range in each layer. Further, in the example of AlexNet using FLOAT16, 80% of the erroneous values that lead to SDCs lie outside this range, while only 9.67% of the erroneous values that lead to benign outcomes do so. Similar trends are found in AlexNet, CaffeNet, and NiN using DOUBLE, FLOAT, FLOAT16, and 32b_rb10. This is because the data types provide more dynamic value range than the networks need. The redundant value ranges lead to larger value deviation under faults and are more vulnerable to SDCs. This indicates that we can leverage symptom-based detectors to detect SDCs when these data types are used (Section 6.2). On the other hand, 16b_rb10 and 32b_rb26

suppress the maximum dynamic value ranges. ConvNet is an exception: ConvNet has a limited number of outputs and a small stack of layers, as even a small perturbation in values may significantly affect the output rankings.

5.1.4 Layer Position and Type. To investigate how errors in different layers propagate through the network, we study the error sensitivity of both the positions and types of layers. We show the SDC probability per layer, ordered by the position for AlexNet, CaffeNet, and NiN in Figure 6a and for ConvNet in Figure 6b.

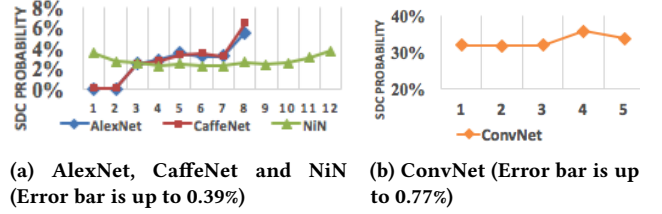


Figure 6: SDC probability per layer using FLOAT16, Y-axis is SDC probability and X-axis is layer position

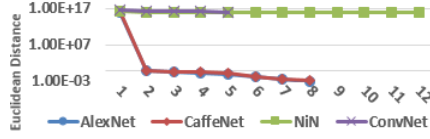
In Figure 6a, in AlexNet and CaffeNet, we observed very low SDC probabilities in the first and second layers, compared to the other layers. The reason is the Local Response Normalization (LRN) layers implemented at the end of the first and second layers in these networks normalize the faulty values, thus mitigating the effect of large deviations in the values. However, there is no LRN or similar normalization layer in the other layers. NiN and ConvNet do not have such a normalization layer, and hence, NiN (in Figure 6a) and ConvNet (in Figure 6b) have a relatively flat SDC probability across all convolutional layers (layers 1 to 12 in NiN and layer 1 to layer 3 in ConvNet). We also observe there is an increase in the SDC probabilities in layers in AlexNet and CaffeNet after the LRNs. This is because the later layers require narrower value ranges (Table 4), and hence wider value ranges and bits are likely to result in SDCs. Note that the fully-connected layers in AlexNet (layer 6 to layer 8), CaffeNet (layer 6 to layer 8), and ConvNet (layers 4 and 5) have higher SDC probabilities. This is because (1) they are able to directly manipulate the ranking of the output candidates, and (2) ACTs are fully-connected, and hence faults spread to all ACTs right away and have much higher impact on the final outputs. Recall that there is no fully-connected layer in NiN, however, and hence this effect does not occur.

To further illustrate the effect of LRN on mitigating error propagation, we measured the average Euclidean distance between the ACT values in the fault injection runs and the golden runs at the end of each layer after faults are injected at the first layer in different networks using the DOUBLE data type. The results are shown in Figure 7. We choose the DOUBLE data type for this experiment as it accentuates any differences due to its wide value range. As we can see, the Euclidean distance decreases sharply from the first layer to the second layer after LRN in AlexNet and CaffeNet. However, neither NiN nor ConvNet implement LRN or similar layers, and hence the Euclidean distances at each layer are relatively flat.

Recall that the POOL and ReLU layers are implemented in all four networks we consider, and are placed at the end of each convolutional and fully-connected layer after MACs. Recall also that POOL

Table 4: Value range for each layer in different networks in the error-free execution

Network	Layer 1	Layer 2	Layer 3	Layer 4	Layer 5	Layer 6	Layer 7	Layer 8	Layer 9	Layer 10	Layer 11	Layer 12
AlexNet	-691.813 662.505	-228.296 224.248	-89.051 98.62	-69.245 145.674	-36.4747 133.413	-78.978 43.471	-15.043 11.881	-5.542 15.775	N/A	N/A	N/A	N/A
CaffeNet	-869.349 608.659	-406.859 156.569	-73.4652 88.5085	-46.3215 85.3181	-43.9878 155.383	-81.1167 38.9238	-14.6536 10.4386	-5.81158 15.0622	N/A	N/A	N/A	N/A
NiN	-738.199 714.962	-401.86 1267.8	-397.651 1388.88	-1041.76 875.372	-684.957 1082.81	-249.48 1244.37	-737.845 940.277	-459.292 584.412	-162.314 437.883	-258.273 283.789	-124.001 140.006	-26.4835 88.1108
ConvNet	-1.45216 1.38183	-2.16061 1.71745	-1.61843 1.37389	-3.08903 4.94451	-9.24791 11.8078	N/A	N/A	N/A	N/A	N/A	N/A	N/A

**Figure 7: Euclidean distance between the erroneous values and correct values of all ACTs at each layer of networks using DOUBLE, Y-axis is Euclidean distance and X-axis is layer position (Faults are injected at layer 1)**

picks the local maximum ACT value and discards the rest of the ACTs before forwarding them to the next layer, while ReLU resets values to zero if the value is negative. Since POOL and ReLU can either discard or completely overwrite the values, they can mask errors in different bits. Therefore, we study the bit-wise SDC probability (or error propagation rate) per layer after each POOL or ReLU structure in convolutional layers in Table 5. We measured this rate by comparing the ACT values bit by bit at the end of the last layer. Due to space constraints, we only show the result of AlexNet using FLOAT16, though similar results were observed in the other cases.

Table 5: Percentage of bit-wise SDC across layers in AlexNet using FLOAT16 (Error bar is from 0.2% to 0.63%)

Layer 1	Layer 2	Layer 3	Layer 4	Layer 5
19.38%	6.20%	8.28%	6.08%	1.63%

There are three main observations in Table 5: (1) In general, there is a decreasing propagation probability across layers, as faults that occur in earlier layers have a higher probability of propagating to other layers and spreading. (2) Even through many faults spread into multiple locations and reach the last layer, only a small fraction of them (5.5% on average, compared with AlexNet in Figure 6a) will affect the final ranking of the output candidates. The reason, as explained in Section 5.1.3, is that the numerical value of ACTs affected by faults is a more influential factor affecting the SDC probability than the number of erroneous ACTs. (3) A majority of the faults (84.36% on average) are masked by either POOL or ReLU during the propagation and cannot even reach the last layer. Therefore, error detection techniques that are designed to detect bit-wise mismatches (i.e., DMR) may detect many errors that ultimately get masked.

5.1.5 Datapath FIT rate. We calculate the datapath FIT rates for different networks using each datatype based on the canonical model of datapath in Figure 1b, and the formula in Eq. 1. Note that the latches assumed in between execution units are the minimum

sets of latches to implement the units, so our calculations of datapath FIT rate are conservative. The results are listed in Table 6. As seen, the FIT rate varies a lot depending on the network and data type used. For example, it ranges from 0.004 to 0.84 in NiN and ConvNet using 16b_rb10, and from 0.002 to 0.42 in AlexNet using 16b_rb10 and 32b_rb10. Depending on the design of the DNN accelerator and the application, the datapath's FIT rate may exceed the FIT budget allowed for the DNN accelerator and will hence need to be protected. We will further discuss this in Section 6.1.

Table 6: Datapath FIT rate in each data type and network

	ConvNet	AlexNet	CaffeNet	NiN
FLOAT	1.76	0.02	0.03	0.10
FLOAT16	0.91	0.009	0.009	0.008
32b_rb26	1.73	0.002	0.005	0.002
32b_rb10	2.45	0.42	0.41	0.54
16b_rb10	0.84	0.002	0.007	0.004

5.2 Buffer Faults: A Case Study on Eyeriss

Eyeriss [13] is a recently proposed DNN accelerator whose component parameters are publicly available. We use Eyeriss in this case study - the reason is articulated in Section 4.2. Other than the components shown in Figure 1, Eyeriss implements a *Filter SRAM*, *Img REG* and *PSum REG* on each PE for data reuses listed in Table 1. The details of the dataflow are described in Chen et al. [13]. We adopted the original parameters of the Eyeriss microarchitecture at 65 nm and projected it to 16nm technology. For the purpose of this study, we simply scale the components of Eyeriss in proportion to process technology generation improvements, ignoring other architectural issues. In Table 7, we list the microarchitectural parameters of Eyeriss at the original 65nm and the corresponding projections at 16nm. We assume a scaling factor of 2 for each technology generation, and as there are 4 generations between 65nm and 16nm technology (based on published values by the TSMC foundry), we scaled up the number of PEs and the sizes of buffers by a factor of 8. In the rest of this work, we use the parameters of Eyeriss at 16nm.

Table 7: Parameters of microarchitectures in Eyeriss (Assuming 16-bit data width, and a scaling factor of 2 for each technology generation)

Feature Size	No. of PE	Size of Global Buffer	Size of One Filter SRAM	Size of One Img REG	Size of One PSum REG
65nm	168	98KB	0.344KB	0.02KB	0.05KB
16nm	1,344	784KB	3.52KB	0.19KB	0.38KB

5.2.1 Data Reuse and Buffer. Here we measure and compare SDC probabilities of different buffers in Eyeriss by randomly injecting 3,000 faults in each buffer component for different network

parameters. By analyzing the results, we found that faults in buffers exhibit similar trends as datapath faults for each parameter of data type, network, value, layer, though the absolute SDC probabilities and FIT rates are different (usually higher than for datapath faults due to the amount of reuse and size of the components). Hence, we do not repeat these sensitivity results in this section. Rather, we present SDC probabilities and FIT rates for each buffer of the different networks in Table 8. The calculation of the FIT rate is based on Eq. 1. We show the results using the 16b_rb10 data type as a 16-bit FxP data type is implemented in Eyeriss.

Table 8: SDC probability and FIT rate for each buffer component in Eyeriss (SDC probability / FIT Rate)

Network	Global Buffer	Filter SRAM	Img REG	PSum REG
ConvNet	69.70%/87.47	66.37%/62.74	70.90%/3.57	27.98%/2.82
AlexNet	0.16%/0.20	3.17%/3.00	0.00%/0.00	0.06%/0.006
CaffeNet	0.07%/0.09	2.87%/2.71	0.00%/0.00	0.17%/0.02
NiN	0.03%/0.04	4.13%/3.90	0.00%/0.00	0.00%/0.00

As seen, as the network becomes deeper, its buffers are much more immune to faults. For example, ConvNet is less deep than the other three networks, and the FIT rate of *Global Buffer* and *Filter SRAM* are respectively 87.47 and 62.74, compared to 0.2 and 3.0 for AlexNet. This sensitivity is consistent with datapath faults. Another observation is that *Img REG* and *PSum REG* have relatively low FIT rates as they both have smaller component sizes and a short time window for reuse: a faulty value in *Img REG* will only affect a single row of fmap and only the next accumulation operation if in *PSum REG*. Finally, we find that buffer FIT rates are usually a few orders of magnitude higher than datapath FIT rates, and adding these buffers for reuse dramatically increases the overall FIT rate of DNN accelerators. The reasons are twofold: (1) Buffers by nature have larger sizes than the total number of latches in the datapath, and (2) due to reuse, the same fault can be read multiple times and lead to the spreading of errors to multiple locations in a short time, resulting in more SDCs. Both lead to a higher FIT rate (See in Eq. 1). We will further discuss its implication in Section 6.1.

6 MITIGATION OF ERROR PROPAGATION

We explore three directions to mitigate error propagation in DNN systems based on the results in the previous section. First, we discuss the reliability implications in designing DNN systems. Second, we adapt a previously proposed software based technique, *Symptom-based Error Detectors (SED)*, for detecting errors in DNN-based systems. Finally, we use a recently proposed hardware technique, *Selective Latch Hardening (SLH)* to detect and correct datapath faults. Both techniques leverage the observations made in the previous section and are optimized for DNNs.

6.1 Implications to Resilient DNN Systems

(1) **Data Type:** Based on our analysis in Section 5.1, we can conclude that DNNs should use data types that provide just-enough numeric value range and precision required to operate the target DNNs. For example, in Table 6, we found that the FIT rate of datapath can be reduced by more than two orders of magnitude if we replace type 32b_rb10 with type 32b_rb26 (from 0.42 to 0.002).

However, existing DNN accelerators tend to follow a *one-size-fits-all* approach by deploying a data type representation which is

long enough to work for all computations in different layers and DNNs [12, 13, 19]. Therefore, it is not always possible to eliminate redundant value ranges that the data type provides across layers and DNNs. The redundant value ranges are particularly vulnerable to SDCs as they tend to cause much larger value deviations (Section 5.1.2). We propose a low-cost symptom-based error detector that detects errors caused by the redundant value ranges regardless of whether conservative data types are used. A recent study has proposed a reduced precision protocol which stores data in shorter representations in memory and unfolds them when in the datapath to save energy [30]. The approach requires hardware modifications and may not be always supported in accelerators. We defer the reliability evaluation of the proposed protocol to our future work.

(2) **Sensitive Bits:** Once a restricted data type is used for a network, the dynamic value range is suppressed, mitigating SDCs caused by out-of-range values. However, the remaining SDCs can be harder to detect as erroneous values hide in normal value ranges of the network. Fortunately, we observe that the remaining SDCs are also caused by bit-flips at certain bit positions (i.e., high bit positions in FxP) (Section 5.1.2). Hence, we can selectively harden these bits to mitigate the SDCs (Section 6.3).

(3) **Normalization Layers:** The purpose of the normalization layers such as the LRN layer is to increase the accuracy of the network [31]. In Section 5.1.4, we found that LRN also increases the resilience of the network as it normalizes a faulty value with its adjacent fault-free values across different fmaps to mitigate SDCs. Therefore, one should use such layers if possible. Further, one should place error detectors after such layers to leverage the masking opportunities, thus avoiding detecting benign faults.

(4) **Data Reuse:** Recently, multiple dataflows and architectures have been proposed and demonstrated to provide both energy and performance improvements [12, 13]. However, adding these local buffers implementing more sophisticated dataflow dramatically increases the FIT rate of a DNN accelerator. For example, the FIT rate of *Filter SRAMs* (3.9 in NiN, Table 8) can be nearly 1000x higher than the FIT rate of the entire datapath (0.004 in NiN, Table 8). Unfortunately, however, protecting small buffers through ECC may incur very high overheads due to smaller read granularities. We propose an alternative approach, SED, to protect these buffers at low cost (Section 6.2).

(5) **Datapath Protection:** From Table 6, we found the datapath FIT rate alone can go up to 2.45 without careful design, or 0.84 even with a resilient data type (16b_rb10, in ConvNet). The safety standard, for example in ISO 26262, mandates the overall FIT rate of the SoC carrying DNN accelerator to be less than 10 FIT. Since a DNN accelerator is often a very small area fraction of the total on the SoC. The FIT budget allocated to the DNN accelerator should be only a tiny fraction of 10. Hence, datapath faults cannot be ignored as they stretch the FIT budget allocated to the DNN accelerator.

6.2 Symptom-based Error Detectors (SED)

A symptom-based detector is an error detector that leverages application-specific symptoms under faults to detect anomalies. Examples of symptoms are unusual values of variables [26, 42], numbers of loop iterations [26, 35], or address spaces accessed by the program [35, 42]. For the proposed detector, we use the value ranges of ACTs as the symptom to detect SDC-causing faults. This is based on

the observation from Section 5.1.3: *If an error makes the magnitude of ACTs very large, it likely leads to an SDC, and if it does not, it is likely to be benign.* In the design of the error detector, there are two questions that need to be answered: *Where* (which program locations) and *What* (which reference value ranges) to check? The proposed detector consists of two phases - we describe each phase along with the answers to the two questions below:

Learning: Before deploying the detector, a DNN application needs to be instrumented and executed with its representative test inputs to derive the value ranges in each layer during the fault-free execution. We can use these value ranges, say $-X$ to Y , as the bounds for the detector. However, to be safe, we apply an additional 10% cushion on top of the value ranges of each layer, that is $(-1.1 \cdot X)$ to $(1.1 \cdot Y)$ as the reference values for each detector to reduce false alarms. Note that the learning phase is only required to be performed once before the deployment.

Deployment: Once the detectors are derived, they are checked by the host which off-loads tasks to the DNN accelerator. At the end of each layer, the data of fmaps of the current layer are calculated and transferred to the global buffer from the PE array as the input data of ifmaps for the next layer. These data will stay in the global buffer during the entire execution of the next layer for reuse. This gives us an opportunity to execute the detector asynchronously from the host, and check the values in global buffer to detect errors. We perform the detection asynchronously to keep the runtime overheads as low as possible.

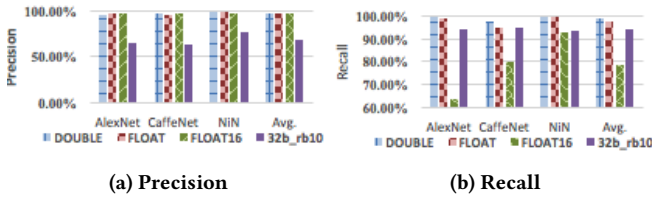


Figure 8: Precision and recall of the symptom-based detectors across networks (Error bar is from 0.03% to 0.04%)

Evaluation: After deploying the detector, we measure its coverage by randomly injecting 3,000 single bit-flip faults in each hardware component, using all 3 FP data types and 32b_rb10 in AlexNet, CaffeNet and NiN, one fault per fault injection run. As we explained earlier, we do not include the 16b_rb10 and 32b_rb26 data types or the ConvNet network as they do not exhibit strong symptoms, and hence symptom-based detectors are unlikely to provide high coverage in these cases. So there are a total of $3,000 \cdot 5 \cdot 4 \cdot 3 = 180,000$ faults injected for this experiment.

We define two metrics in our evaluation: (1) Precision: $1 - (\text{The number of benign faults that are detected by the detector as SDC}) / (\text{The number of faults injected})$, and (2) Recall: $(\text{The number of SDC-causing faults that are detected by the detector}) / (\text{The number of total SDC-causing faults})$. The results are shown in Figure 8a and Figure 8b for the precision and the recall respectively averaged across the data types and components (due to space constraints, we only show the average values). As can be seen, the average precision is 90.21% and the average recall is 92.5%. Thus, we can reduce the FIT rates of Eyeriss using FLOAT and FLOAT16 by 96%

(from 8.55 to 0.35) and 70% (from 2.63 to 0.79) respectively using the symptom-based detector technique (based on Equation 1).

6.3 Selective Latch Hardening (SLH)

Latch hardening is a hardware error mitigation technique that adds redundant circuitry to sequential storage elements (i.e., latches) to make them less sensitive to errors. Protecting the latches in the datapath can be vital for highly dependable systems as they become the reliability bottleneck once all buffers are protected (e.g., by ECCs). Given that the technology keeps scaling to smaller feature sizes [5, 16], it will be more important to mitigate datapath faults in the future. There have been a number of different hardened latch designs that differ in their overheads and levels of protection, and latch hardening need not be applied in an all-or-nothing manner. For example, Sullivan et al. [54] developed an analytical model for hardened latch design space exploration and demonstrated cost-effective protection by hardening only the most sensitive latches and by combining hardening techniques offering differing strengths in an error-sensitivity proportional manner. Since we observed and characterized asymmetric SDC sensitivity in different bits in Section 5.1.2, we can leverage this model to selectively harden each latch using the most efficient hardening technique to achieve sufficient error coverage at a low cost.

Design Space Exploration: There are a wide variety of latch hardening techniques that vary in their level of protection and overheads. Table 9 shows the three hardening techniques used by [54]; these same techniques are considered in this paper, though the methodology should apply with any available hardened latches. The baseline design in the table refers to an unprotected latch.

Table 9: Hardened latches used in design space exploration

Latch Type	Area Overhead	FIT Rate Reduction
Baseline	1x	1x
Strike Suppression (RCC)	1.15x	6.3x
Redundant Node (SEUT)	2x	37x
Triplicated (TMR)	3.5x	1,000,000x

Evaluation: Figure 9a shows the AlexNet FIT rate reduction versus the fraction of protected latches assuming a perfect hardening technique that completely eliminates errors. We plot this curve to illustrate the maximum benefit one can achieve by protecting bits that are more sensitive to SDC with priority. β characterizes the asymmetry of SDC FIT rate in different bits (latches)—a high β indicates that a small number of latches dictate the overall SDC probability. As can be seen, there are negative exponential curves in the figure, such that we can selectively protect only the most sensitive latches for area-efficient SDC reduction.

Figure 9b and Figure 9c show the AlexNet FIT rate reduction versus the latch area overhead when using each hardened latch, and the optimal combination of the hardened designs (*Multi*) generated by the model. Due to space constraints, we only show the AlexNet result for the FLOAT16 and 16b_rb10 data types (the other networks and data types exhibit similar trends). By exploiting the asymmetry of error sensitivity in data type bits and combining complementary hardening techniques, one can achieve significant protection while paying only modest area costs. For example, applying the three hardening techniques together can reduce the latch FIT rate by

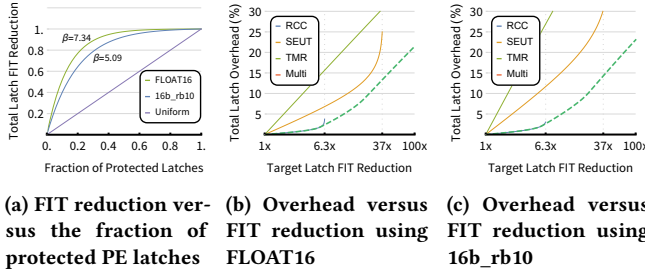


Figure 9: Selective Latch Hardening for the Eyeriss Accelerator running AlexNet

100x, while incurring about 20% and 25% latch area overheads in FLOAT16 and 16b_rb10, respectively. This translates to a chip-level area overhead roughly akin to that required for ECC protection of the larger (and more easily protected) SRAM structures.

7 RELATED WORK

There were a few studies years ago on the fault tolerance of neural networks [1, 3, 44]. While these studies performed fault injection experiments on neural networks and analyzed the results, the networks they considered had very different topologies and many fewer operations than today’s DNNs. Further, these studies were neither in the context of the safety critical platforms such as self-driving cars, nor did they consider DNN accelerators for executing the applications. Hence, they do not provide much insight about error propagation in modern DNN systems.

Reis et al. [46] and Oh et al. [40] proposed software techniques that duplicate all instructions to detect soft errors. Due to the high overheads of these approaches, researchers have investigated selectively targeting the errors that are important to an application. For example, Li et al. [35, 36] characterized error propagation patterns in software applications on CPUs and GPUs and devised efficient protection techniques. Hari et al. [26] analyzed popular benchmarks and designed application-specific error detectors. Feng et al. [20] proposed a static analysis method to identify vulnerable parts of the applications for protection. Lu et al. [38] identified SDC-prone instructions to protect using a decision tree classifier, while Laguna et al. [32] used a machine learning approach to identify sensitive instructions in scientific applications. While these techniques are useful to mitigate soft errors in general purpose applications, they cannot be easily applied to DNN systems which implement a different instruction set and operate on a specialized microarchitecture.

Many studies [12, 13, 25] proposed novel microarchitectures for accelerating DNN applications. These studies only consider the performance and energy overheads of their designs and do not consider reliability. In recent work, Fernandes et. al. [21] evaluated the resilience of histogram of oriented gradient applications for self-driving cars, but they did not consider DNNs. Reagan et.al. [45] and Chatterjee et.al. [11] explored energy-reliability limits of DNN systems, but they focused on different networks and fault models.

The closest related work is by Temam et. al. [55], which investigated the error resilience of neural network accelerators at the transistor-level. Our work differs in three aspects: (1) Their work

assumed a simple neural network prototype, whereas we investigate modern DNN topologies. (2) Their work does not include any sensitivity study and is limited to the hardware datapath of a single neural network accelerator. Our work explores the resilience sensitivity to different hardware and software parameters. (3) Their work focused on permanent faults, rather than soft errors. Soft errors are separately regulated by ISO 26262, and hence we focus on them.

8 CONCLUSION

DNNs (Deep Neural Networks) have gained prominence in recent years and they are being deployed on hardware accelerators in self-driving cars for real-time image classification. In this work, we characterize the impact of soft errors on DNN systems through a large-scale fault injection experiment with 4 popular DNNs running on a recently proposed DNN hardware accelerator. We find that the resilience of a DNN system depends on the data types, values, data reuse, and the types of layers in the design. Based on these insights, we formulate guidelines for designing resilient DNN systems and propose two efficient DNN protection techniques to mitigate soft errors. We find that the techniques significantly reduce the rate of Silent Data Corruption (SDC) in DNN systems with acceptable performance and area overheads.

9 ACKNOWLEDGEMENTS

We thank the anonymous reviewers of SC’17 for their comments that helped improve the paper. This work was supported in part by a Discovery Grant from the Natural Science and Engineering Research Council (NSERC), Canada.

REFERENCES

- [1] Alippi, Cesare, Vincenzo Piuri, and Mariagiovanna Sami. 1995. Sensitivity to errors in artificial neural networks: A behavioral approach. *IEEE Transactions on Circuits and Systems I: Fundamental Theory and Applications* (1995).
- [2] Autonomous car facts 2016. Keynote: Autonomous Car A New Driver for Resilient Computing and Design-for-Test. (2016). Retrieved Oct. 2016 from https://nepp.nasa.gov/workshops/etw2016/talks/15WED/20160615-0930-Autonomous_Saxena-Nirmal-Saxena-Rec2016Jun16-nasaNEPP.pdf
- [3] Bettola, Simone, and Vincenzo Piuri. 1998. High performance fault-tolerant digital neural networks. *IEEE transactions on computers* (1998).
- [4] Bojarski, Mariusz, Davide Del Testa, Daniel Dworakowski, Bernhard Firner, Beat Flepp, Prasoon Goyal, Lawrence D. Jackel and others. 2016. End to End Learning for Self-Driving Cars. *arXiv preprint arXiv:1604.07316* (2016).
- [5] Borkar, Shekhar. 2005. Designing reliable systems from unreliable components: the challenges of transistor variability and degradation. In *Proceedings of the International Symposium on Microarchitecture (MICRO)*, Vol. 25. 10–16.
- [6] BVCL 2014. BERKELEY VISION AND LEARNING CENTER. (2014). Retrieved Oct. 2016 from <http://bvcl.eecs.berkeley.edu>
- [7] Caffe Model 2014. Caffe Model Zoo. (2014). Retrieved Oct. 2016 from http://caffe.berkeleyvision.org/model_zoo.html
- [8] CaffeNet 2014. CaffeNet. (2014). Retrieved Oct. 2016 from http://caffe.berkeleyvision.org/model_zoo.html
- [9] Cavigelli, Lukas, David Gschwend, Christoph Mayer, Samuel Willi, Beat Muheim, and Luca Benini. 2015. Origami: A convolutional network accelerator. In *In Proceedings of the 25th edition on Great Lakes Symposium on VLSI*.
- [10] Chakradhar, Srimat, Murugan Sankaradas, Venkata Jakkula, and Srihari Cadambi. 2010. A dynamically configurable coprocessor for convolutional neural networks. In *ACM SIGARCH Computer Architecture News*.
- [11] Chatterjee, Avhishek, and Lav R. Varshney. 2017. Energy-reliability limits in nanoscale neural networks. In *The 51st Annual Conference on Information Sciences and Systems (CISS)*. 1–6.
- [12] Chen, Tianshi, Zidong Du, Ninghui Sun, Jia Wang, Chengyong Wu, Yunji Chen, and Olivier Temam. 2014. Dianao: A small-footprint high-throughput accelerator for ubiquitous machine-learning. In *ACM Sigplan Notices*.
- [13] Chen, Yu-Hsin, Joel Emer, and Vivienne Sze. 2016. Eyeriss: A spatial architecture for energy-efficient dataflow for convolutional neural networks. In *Proceedings of the International Symposium on Computer Architecture (ISCA)*. 367–379.

- [14] Chen, Yunji, Tao Luo, Shaoli Liu, Shijin Zhang, Liqiang He, Jia Wang, Ling Li and others. 2014. Dadiannao: A machine-learning supercomputer. In *Proceedings of the International Symposium on Microarchitecture (MICRO)*.
- [15] CIFAR dataset 2014. CIFAR-10. (2014). Retrieved Oct. 2016 from <https://www.cs.toronto.edu/~kriz/cifar.html>
- [16] Constantinescu, Cristian. 2008. Intermittent faults and effects on reliability of integrated circuits. In *Proceedings of the Reliability and Maintainability Symposium*. 370.
- [17] ConvNet 2014. High-performance C++/CUDA implementation of convolutional neural networks. (2014). Retrieved Oct. 2016 from <https://code.google.com/p/cuda-convnet>
- [18] Dahl, George E., Dong Yu, Li Deng, and Alex Acero. 2012. Context-dependent pre-trained deep neural networks for large-vocabulary speech recognition. *IEEE Transactions on Audio, Speech, and Language Processing* 20, 1 (2012), 30–42.
- [19] Du, Zidong, Robert Fasthuber, Tianshi Chen, Paolo Ienne, Ling Li, Tao Luo, Xiaobing Feng, Yunji Chen, and Olivier Temam. 2015. ShiDianNao: shifting vision processing closer to the sensor. In *ACM SIGARCH Computer Architecture News*.
- [20] Feng, Shuguang and Gupta, Shantanu and Ansari, Amin and Mahlke, Scott. 2010. Shoestring: probabilistic soft error reliability on the cheap. In *ACM SIGARCH Computer Architecture News*, Vol. 38. ACM, 385–396.
- [21] Fernandes, Fernando and Weigel, Lucas and Jung, Claudio and Navaux, Philippe and Carro, Luigi and Rech, Paolo. 2016. Evaluation of histogram of oriented gradients soft errors criticality for automotive applications. *ACM Transactions on Architecture and Code Optimization (TACO)* 13, 4 (2016), 38.
- [22] Gill, B., N. Seifert, and V. Zia. 2009. Comparison of alpha-particle and neutron-induced combinational and sequential logic error rates at the 32nm technology node. In *Proceedings of the International Reliability Physics Symposium (IRPS)*.
- [23] Gokhale, Vinayak, Jonghoon Jin, Aysegul Dundar, Berin Martini, and Eugenio Culurciello. 2014. A 240 g-ops/s mobile coprocessor for deep neural networks. In *Proceedings of the IEEE Conference on Computer Vision and Pattern Recognition Workshops*.
- [24] Gupta, Suyog, Ankur Agrawal, Kailash Gopalakrishnan, and Prithish Narayanan. 2015. Deep learning with limited numerical precision. (2015).
- [25] Han, Song, Xingyu Liu, Huizi Mao, Jing Pu, Ardavan Pedram, Mark A. Horowitz, and William J. Dally. 2016. EIE: efficient inference engine on compressed deep neural network. (2016).
- [26] Hari, Siva Kumar Sastry and Adve, Sarita V and Naeimi, Helia. 2012. Low-cost program-level detectors for reducing silent data corruptions. In *Proceedings of the International Conference on Dependable Systems and Networks (DSN)*.
- [27] He, Kaiming, Xiangyu Zhang, Shaoqing Ren, and Jian Sun. 2015. Deep residual learning for image recognition. *Proceedings of the IEEE conference on computer vision and pattern recognition* (2015).
- [28] IEC 61508 2016. Functional Safety and IEC 61508. (2016). Retrieved Oct. 2016 from <http://www.iec.ch/functionalsafety/>
- [29] ImageNet 2014. ImageNet. (2014). Retrieved Oct. 2016 from <http://image-net.org>
- [30] Judd, Patrick, Jorge Albericio, Tayler Hetherington, Tor M. Aamodt, Natalie Enright Jerger, and Andreas Moshovos. 2016. Proteus: Exploiting Numerical Precision Variability in Deep Neural Networks.
- [31] Krizhevsky, Alex, Ilya Sutskever, and Geoffrey E. Hinton. 2012. Imagenet classification with deep convolutional neural networks. In *Advances in neural information processing systems*.
- [32] Laguna, Ignacio, Martin Schulz, David F. Richards, Jon Calhoun, and Luke Olson. 2016. Ipas: Intelligent protection against silent output corruption in scientific applications. In *Proceedings of the International Symposium on Code Generation and Optimization (CGO)*.
- [33] Lane, Nicholas D., and Petko Georgiev. 2015. Can deep learning revolutionize mobile sensing?. In *Proceedings of the 16th International Workshop on Mobile Computing Systems and Applications*.
- [34] LeCun, Yann, Koray Kavukcuoglu, and Clément Farabet. 2010. Convolutional networks and applications in vision.. In *Proceedings of IEEE International Symposium on Circuits and Systems*.
- [35] Li, Guanpeng and Lu, Qining and Pattabiraman, Karthik. 2015. Fine-Grained Characterization of Faults Causing Long Latency Crashes in Programs. In *Proceedings of the International Conference on Dependable Systems and Networks (DSN)*.
- [36] Li, Guanpeng and Pattabiraman, Karthik and Cher, Chen-Yong and Bose, Pradip. 2016. Understanding Error Propagation in GPGPU Applications. In *Proceedings of the International Conference on High Performance Computing, Networking, Storage and Analysis (SC)*.
- [37] Lin, Min and Chen, Qiang and Yan, Shuicheng. 2013. Network in network. *arXiv preprint arXiv:1312.4400* (2013).
- [38] Lu, Qining and Li, Guanpeng and Pattabiraman, Karthik and Gupta, Meeta S and Rivers, Jude A. 2017. Configurable detection of SDC-causing errors in programs. *ACM Transactions on Embedded Computing Systems (TECS)* 16, 3 (2017), 88.
- [39] Neale, Adam, and Manoj Sachdev. 2016. Neutron Radiation Induced Soft Error Rates for an Adjacent-ECC Protected SRAM in 28 nm CMOS. (2016).
- [40] Oh, Nahmsuk, Philip P. Shirvani, and Edward J. McCluskey. 2002. Error detection by duplicated instructions in super-scalar processors. *IEEE Transactions on Reliability* (2002).
- [41] Park, Seongwook, Kyeongryeol Bong, Dongjoo Shin, Jinmook Lee, Sungpill Choi, and Hoi-Jun Yoo. [n. d.]. 4.6 A1. 93TOPS/W scalable deep learning/inference processor with tetra-parallel MIMD architecture for big-data applications. In *International Solid-State Circuits Conference*.
- [42] Karthik Pattabiraman, Giancinto Paolo Saggese, Daniel Chen, Zbigniew Kalbarczyk, and Ravishankar Iyer. 2011. Automated derivation of application-specific error detectors using dynamic analysis. *IEEE Transactions on Dependable and Secure Computing* 8, 5 (2011), 640–655.
- [43] Peemen, Maurice, Arnaud AA Setio, Bart Mesman, and Henk Corporaal. 2013. Memory-centric accelerator design for convolutional neural networks. In *IEEE 31st International Conference on Computer Design (ICCD)*.
- [44] Piuri, Vincenzo. 2001. Analysis of fault tolerance in artificial neural networks. *J. Parallel and Distrib. Comput.* (2001).
- [45] Reagen, Brandon and Whatmough, Paul and Adolf, Robert and Rama, Saketh and Lee, Hyunkwang and Lee, Sae Kyu and Hernández-Lobato, José Miguel and Wei, Gu-Yeon and Brooks, David. 2016. Minerva: Enabling low-power, highly-accurate deep neural network accelerators. In *Proceedings of the International Symposium on Computer Architecture (ISCA)*. 267–278.
- [46] Reis, George A., Jonathan Chang, Neil Vachharajani, Ram Rangan, and David I. August. 2005. SWIFT: Software implemented fault tolerance. In *Proceedings of the International Symposium on Code Generation and Optimization (CGO)*.
- [47] Russakovsky, Olga, Jia Deng, Hao Su, Jonathan Krause, Sanjeev Satheesh, Sean Ma, Zhiheng Huang and others. 2015. Imagenet large scale visual recognition challenge. *International Journal of Computer Vision* 115, 3 (2015), 211–252.
- [48] Safety Standard 2016. ISO-26262: Road Vehicles Functional safety. (2016). Retrieved Oct. 2016 from https://en.wikipedia.org/wiki/ISO_26262
- [49] Sankaradas, Murugan, Venkata Jakkula, Srihari Cadambi, Srimat Chakradhar, Igor Durdanovic, Eric Cosatto, and Hans Peter Graf. 2009. A massively parallel coprocessor for convolutional neural networks. In *IEEE International Conference on Application-specific Systems, Architectures and Processors*.
- [50] Seifert, Norbert, Balkaran Gill, Shah Jahinuzzaman, Joseph Basile, Vinod Ambrose, Quan Shi, Randy Allmon, and Arkady Bramnik. 2012. Soft error susceptibilities of 22 nm tri-gate devices. (2012).
- [51] Danny Shapiro. 2016. Introducing Xavier, the NVIDIA AI Supercomputer for the Future of Autonomous Transportation. (2016). Retrieved Apr. 2017 from <https://blogs.nvidia.com/blog/2016/09/28/xavier/>
- [52] Simonyan, Karen, and Andrew Zisserman. 2014. Very deep convolutional networks for large-scale image recognition. *arXiv preprint arXiv:1409.1556* (2014).
- [53] Sriram, Vinay, David Cox, Kuen Hung Tsoi, and Wayne Luk. 2010. Towards an embedded biologically-inspired machine vision processor. In *In Field-Programmable Technology*.
- [54] Sullivan, Michael and Zimmer, Brian and Hari, Siva and Tsai, Timothy and Keckler, Stephen W. 2016. An Analytical Model for Hardened Latch Selection and Exploration. (2016).
- [55] Olivier Temam. 2012. A defect-tolerant accelerator for emerging high-performance applications. In *Proceedings of the International Symposium on Computer Architecture (ISCA)*. 356–367.
- [56] Tiny-CNN [n. d.]. Tiny-CNN Framework. ([n. d.]). Retrieved Oct. 2016 from <https://github.com/nyanp/tiny-cnn>
- [57] Tithi, Jesmin Jahan, Neal C. Crago, and Joel S. Emer. 2014. Exploiting spatial architectures for edit distance algorithms. In *Proceedings of the International Symposium on Performance Analysis of Systems and Software (ISPASS)*.
- [58] TPU [n. d.]. Google supercharges machine learning tasks with TPU custom chip. ([n. d.]). Retrieved Oct. 2016 from <https://cloudplatform.googleblog.com/2016/05/Google-supercharges-machine-learning-tasks-with-custom-chip.html>
- [59] Wei, Jiesheng and Thomas, Anna and Li, Guanpeng and Pattabiraman, Karthik. 2014. Quantifying the accuracy of high-level fault injection techniques for hardware faults. In *Proceedings of the International Conference on Dependable Systems and Networks (DSN)*.
- [60] Yann LeCun. 2000. Deep Learning and the Future of AI. (2000). Retrieved Apr. 2017 from <https://indico.cern.ch/event/510372/>
- [61] Zhang, Chen, Peng Li, Guangyu Sun, Yijin Guan, Bingjun Xiao, and Jason Cong. 2015. Optimizing FPGA-based accelerator design for deep convolutional neural networks. In *Proceedings of ACM/SIGDA International Symposium on Field-Programmable Gate Arrays*.